processes

MDPI

Article

Enhancing Gas Recovery in Tight Dolomite Reservoirs: A Study of Water-Lock Damage and Chemical Drainage

Xiaopeng Yang [1,2], Hongtao Fei [3], Junfeng Shi [1,2], Lianqi Sheng [3], Donghong Guo [1,2] and Erdong Yao [3,*]

[1] Research Institute of Petroleum Exploration and Development, Beijing 100083, China; petroleum126@petrochina.com.cn (X.Y.)
[2] State Key Laboratory of Enhanced Oil Recovery, Beijing 100083, China
[3] State Key Laboratory of Petroleum Resources and Prospecting, China University of Petroleum, Beijing 102249, China; lyc1305220957@163.com (H.F.); 2021216572@student.cup.edu.cn (L.S.)
* Correspondence: yaoed@cup.edu.cn

Abstract: The Lower Paleozoic Ordovician strata within the Ordos Basin harbor dolomite gas reservoirs are characterized by low porosity (0.98% to 14.2%) and low permeability (0.001 mD to 2.8 mD). Gas extraction from these reservoirs is frequently impeded by water lock due to the intrusion of water-based drilling fluids and the accumulation of formation water, which increase water saturation near the wellbore and significantly decrease gas permeability. This research is pivotal in elucidating water-lock mechanisms and developing water-unlocking strategies for such tight gas reservoirs. Comprehensive analysis through wettability tests, spontaneous imbibition, high-speed centrifugal drainage, and nuclear magnetic resonance (NMR) revealed that Jingbian gas field rocks are predominantly water-wet with a spontaneous imbibition water saturation of 60% to 80%, indicating a high propensity for water lock. The pore structure, mainly within the 200 to 300 nm range, presents challenges as high-speed centrifugation achieves only 70% to 80% water saturation displacement, with a drainage rate of about 20% to 30% and a drastic decline in gas permeability by several orders of magnitude. This study identifies the surfactant sodium dodecyl benzene sulfonate (SDBS) as an optimal agent for enhancing water displacement and gas production. At a 0.1% concentration, SDBS improves drainage rate and permeability by 58.5% and 69.42%, respectively, demonstrating its efficacy in mitigating water lock and enhancing recoverability in tight dolomite reservoirs. These findings serve as a scientific guide for augmenting production in similar geological settings.

Keywords: dolomite gas reservoir; water-lock damage; chemical drainage

check for updates

Citation: Yang, X.; Fei, H.; Shi, J.; Sheng, L.; Guo, D.; Yao, E. Enhancing Gas Recovery in Tight Dolomite Reservoirs: A Study of Water-Lock Damage and Chemical Drainage. *Processes* **2023**, *11*, 3228. https://doi.org/10.3390/pr11113228

Academic Editor: Qingbang Meng

Received: 12 October 2023
Revised: 7 November 2023
Accepted: 12 November 2023
Published: 15 November 2023

Copyright: © 2023 by the authors. Licensee MDPI, Basel, Switzerland. This article is an open access article distributed under the terms and conditions of the Creative Commons Attribution (CC BY) license (https://creativecommons.org/licenses/by/4.0/).

1. Introduction

Carbonates play a pivotal role in the global energy landscape, harboring nearly 50% of the world's hydrocarbon resources. The extraction of oil and gas from these formations is a significant contributor to the energy sector, accounting for around 60% of the total hydrocarbon production [1]. The tight carbonate gas reservoirs, a crucial segment of these resources, exhibit a widespread presence, not only across regions such as North America, Russia, and India [2,3] but also within China. Notably, in China, these reservoirs are predominantly situated within the Ordovician strata across several basins, including the Sichuan Basin, the Tarim Basin, North China, and the Ordos Basin. Despite their copious reserves, these basins have not been extensively explored, presenting a substantial potential for future resource development [4,5]. The Ordos Basin, with its Lower Paleozoic Ordovician reservoirs, is particularly noteworthy. These reservoirs are primarily composed of dolomite and are characterized by a complex network of karst caves, micropores, and fractures. This intricate geological composition results in a pronounced heterogeneity, with typically low porosity and permeability indicators [6]. The operational challenge arises when water-based working fluids, utilized during drilling and production, penetrate these hydrophilic reservoirs. The resulting escalation in water saturation correlates inversely with permeability, precipitating a phenomenon known as water-lock damage. This obstruction can diminish or, in severe cases, halt the productivity of gas wells. Consequently, proactive measures such as lock removal and water drainage are imperative for the maintenance of gas production [7,8]

Research delineates water-lock damage as the predominant form of impairment in tight reservoirs, with damage rates soaring to as high as 90% [9–11]. This damage manifests when the initial water saturation falls below the threshold of irreducible water saturation, triggering capillary spontaneous imbibition. The fluid retention effect, which stems from the inflow difficulties of the working fluid, the formation of additional resistance by droplets transitioning from macropores to throats, and the Jamin effect, which involves the obstruction of liquid flow, are identified as principal factors contributing to water-lock damage [12–17]. The tight carbonate gas reservoirs, influenced by their unique sedimentary environments, tend to exhibit lower water saturation levels and pronounced hydrophilicity. The invasion of exogenous water into the primary pore throats poses a severe impediment to gas flow, exacerbating the water-lock dilemma [18,19]. It is, therefore, essential to thoroughly understand the water-lock characteristics of tight carbonate reservoirs and devise suitable strategies for water-lock removal.

To alleviate water lock in tight reservoirs, industry professionals currently employ physical and/or chemical methods. These strategies, which encompass enhancing production pressure differentials, heating the formation, solvent injection, and acid fracturing, aim to diminish liquid-phase saturation and bolster effective gas permeability [16,20–22]. Among these, chemical methods have gained traction, attributed to their specificity and efficacy. The selection of chemical agents, which includes gas-wetting agents such as surfactants, alcohols, fluorocarbon polymers, solid nanoparticles, and nano-emulsions, is governed by considerations of cost and service longevity [23–29]. The underlying mechanism is hypothesized to involve the alteration in near-well zone wettability, reducing both the rock-liquid wettability angle and gas–liquid surface tension, thereby diminishing capillary forces. This approach has proven effective in mitigating damage caused by liquid phase entrapment and in facilitating the removal of water locks. For instance, surfactants are known to significantly reduce interfacial tension [30] and alter wettability towards gas-wetting [31], showcasing promising potential. However, challenges such as adsorption by the formation and environmental concerns remain to be addressed. Notwithstanding the breadth of research on water-unlocking agents in tight sandstone reservoirs, the study of such agents and their corresponding methods in tight carbonate reservoirs is still in its nascent stages.

In the tight carbonate reservoirs of the Ordos Basin, an inverse relationship between gas permeability and water saturation has been observed during well operations and gas production. This trend poses a significant challenge to the normal output of gas wells and necessitates a deeper investigation into the mechanisms of water lock as well as the development of effective water-unlocking techniques. Ensuring the seamless extraction from low-porosity and low-permeability gas reservoirs hinges on the success of these initiatives. This study delves into the wettability characteristics of tight dolomite reservoirs by deploying an array of analytical methods, including contact-angle measurements, spontaneous imbibition tests, high-speed centrifugation, and nuclear magnetic resonance imaging. By examining centrifugal displacement and water saturation under varying drainage pressures and chemical agents, the research aims to unearth the underlying water-unlocking mechanisms and methodologies pertinent to tight carbonate gas reservoirs. The findings underscore the severity of water-lock damage within the Jingbian gas field, where a notably low drainage rate is observed. The application of a 0.1% concentration of the chemical agent sodium dodecyl benzene sulfonate (SDBS) has yielded promising results; the centrifugal drainage rate improved by 58.5%, and gas permeability saw an increase of 69.42%. These improvements are indicative of SDBS's efficacy in enhancing both drainage and gas recovery. The insights gained from this research will significantly contribute to the advancement of gas recovery capabilities in tight carbonate formations, paving the way for more efficient exploitation of these challenging reservoirs.

2. Materials and Methods

2.1. Experimental Materials

1. Experimental cores

The core samples used in the experiment were from Well G24-12#, from which 11 core samples with a length of about 5 cm and a diameter of 2.5 cm were selected for the following experiments, and the experimental cores were labeled as A–K, respectively.

2. Chemical reagents

A 2% KCl brine is used to simulate formation water, and 8 chemical agents are used as water-unlocking reagents. They are four nonionic polyoxyethylene surfactants [AEO-7 (Hai'an Petrochemical Plant, Hai'an, Jiangsu, China), AEO-9 (Hai'an Petrochemical Plant, Hai'an, Jiangsu, China), AM-600 (Mackin Biochemical Co., Ltd., Shanghai, China), and OP-40 (Mackin Biochemical Co., Ltd., Shanghai, China)], two anionic surfactants [sodium dodecyl benzenesulfonate (SDBS) and sodium dodecyl sulfonate (SDS)], and two cationic surfactants [cetyl trimethyl ammonium chloride (CTAC) and octadecyl trimethyl ammonium chloride (OTAC)].

2.2. Analysis of Core Physical Properties

2.2.1. Pore Permeability Measurement

The measurement of core sample dimensions of length and diameter is precisely conducted using vernier calipers after the samples have been thoroughly cleaned and dried. Porosity is determined using a porosity tester, which gauges the void spaces within the core in Figure 1. For permeability testing, a steady-state permeability tester assesses medium to high permeability cores, while a PDP permeability tester is reserved for low-permeability samples where Darcy's law is not applicable in Figure 1. Permeability is then calculated by a computer that automatically records the necessary flow and pressure data.

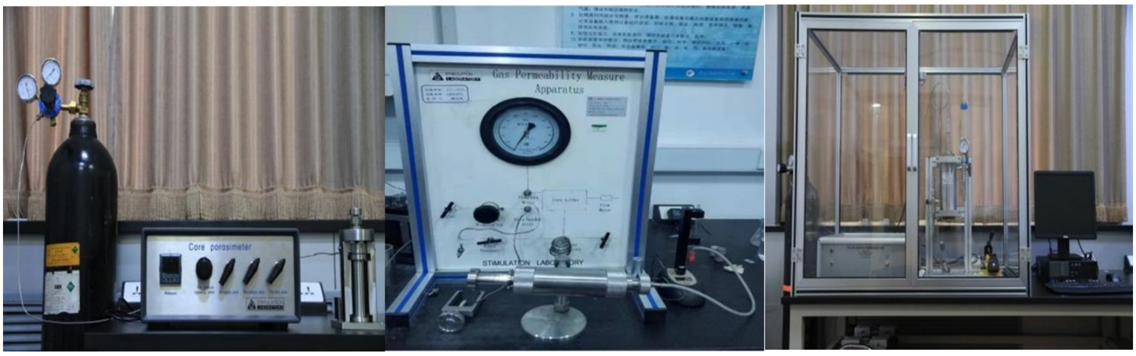

Figure 1. Porosity tester (**left**), permeability tester with steady-state method (**center**), and pulse decay method (**right**).

At the same time, by measuring the permeability of the core before and after solution treatment, the damage rate of the core can be calculated by using the formula.

$$Dr = {k_1 - k_0}/{k_0} \tag{1}$$

where in k_1—permeability after solution treatment; k_0—initial permeability.

2.2.2. Analysis of Rock Mineral Compositions

Test steps: The rock sample intended for analysis is set on the instrument's shelf. Upon activation, the X-ray tube to the left emits X-rays that bathe the sample's surface. The detector positioned on the right captures the diffraction waves reflected by the sample, conveying this information to the connected computer. Each mineral's unique X-ray diffraction pattern is then identified by contrasting the position and intensity of the diffraction lines against a standard reference card, enabling the differentiation of the sample's mineral composition in Figure 2. The parameters of the device are set to Cu target, a diffraction width of DS = SS = 1°, RS = 0.3 mm, a scanning speed of 2000 ($d \cdot min^{-1}$), and a scanning range of 10°–80°.

Figure 2. X-ray diffractometer (model: XRDynamic 500, Anton Paar, Graz, Austria).

2.3. Rock Wettability Analysis

2.3.1. Contact-Angle Method

The rock sample for assessment is placed into the sample pool. The measuring software is executed to adjust the sample pool's height and balance, ensuring the samples are level for clear image acquisition in Figure 3. A microinjector is used to apply precisely 2 µL of water or chemical solutions to the surface of the rock sample to initiate contact. The contact angle is then documented and measured using the software's screenshot functionality, which allows for accurate recording and analysis of the wetting properties of the rock sample.

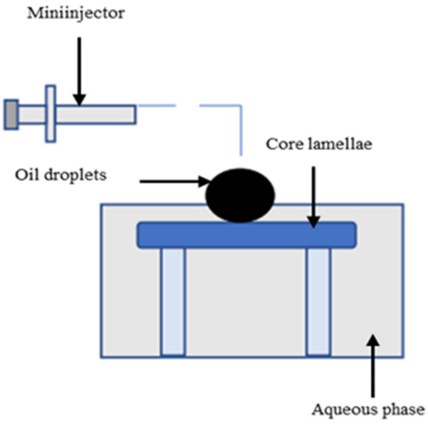

Figure 3. Contact-angle test diagram (model: Theta).

2.3.2. Spontaneous Imbibition Tests

The experimental setup includes a core sample attached to a hanging ring, a beaker, a precision balance, and a data collector in Figure 4. A 200 mL solution is prepared in the beaker, facilitating the diffusion process through capillary action within the pore spaces of the rock. Core samples with a higher porosity and larger pore sizes exhibit faster diffusion rates. The process of infiltration progresses over time from larger to smaller pores, with the rate of penetration decelerating after initial rapid absorption. The weight variations in the core samples resulting from spontaneous imbibition are monitored and recorded by the computer, which provides an accurate depiction of the spontaneous imbibition phenomenon.

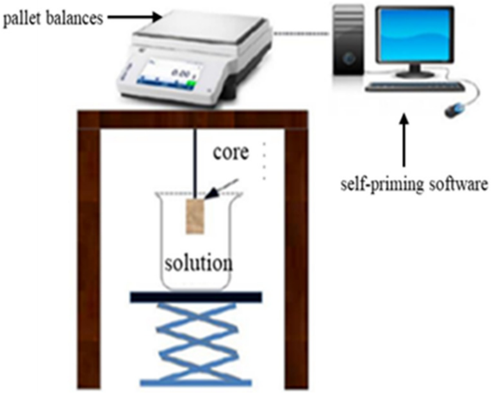

Figure 4. Schematic diagram of core spontaneous imbibition.

2.4. Analysis of Water Saturation and Permeability

The core preparation process involves a two-stage saturation method. Initially, cores are subjected to a vacuum environment for 48 h to ensure the removal of resident air. Subsequent to this, the cores are placed under a water pressure of 15 MPa for another 48 h period to achieve water saturation. Post-saturation, nuclear magnetic resonance (NMR) T_2 spectroscopy scans are conducted to determine the saturation peak area in Figure 5, designated as S_l. The cores are then heated in an oven at 105 °C until a consistent mass indicates no further loss of water, with a stable mass indicating zero water saturation. Following the drying phase, the cores are exposed to either 2% KCl solutions or specific water-unlocking reagents and left to undergo spontaneous imbibition over varying durations. The spontaneous imbibition process is periodically scanned using NMR T_2 spectroscopy to trace changes in water saturation (S_w), calculated using a predefined formula. Here, S_n represents the peak integral area when fully saturated with water, and S_l is the peak integral area during testing.

$$S_w = {}^{S_l}\!/_{S_n} \tag{2}$$

Figure 5. Newman NMR apparatus (model: MacroMR12-150H-I, Niumag Corporation, Suzhou, China).

The permeability under different water saturations was measured by a permeability tester, and the permeability curve under different water saturations was drawn.

2.5. Centrifugal Drainage Experiments

For the evaluation of water distribution within the core samples at various levels of water saturation, the cores are treated until irreducible water saturation is attained. The water distribution within these cores is tested under controlled conditions, with the centrifugal force set at a speed of 3000 revolutions per minute, using a high-speed centrifuge, as depicted in Figure 6.

Figure 6. CSC-12 high-speed centrifugal machine (model: Avanti J-E, Beckman Coulter, Brea, CA, USA).

To ascertain the specifics of the water distribution, NMR T_2 spectrum serves as the primary analytical tool. This method facilitates a detailed understanding of the water phases within the cores' porosity. Additionally, the core samples undergo a pore size calibration process, which employs the mercury injection technique to generate accurate pore size data. This calibration is critical for investigating the distribution and phase of water across different pore sizes under varied pressure and timing conditions, providing insight into the core's hydrophilic characteristics and potential for fluid flow optimization.

2.6. Optimization of Water-Unlocking Reagents

2.6.1. Interfacial Tension Test

The interfacial tension of surfactants was gauged using the du Noüy ring technique at a 0.1% solution concentration. This method involves a platinum ring dipped into the surfactant solution and then lifted away from the liquid's surface, measuring the resistance encountered due to surface tension. The force required to pull the ring from the surface, which includes the weight of the ring and the liquid's surface tension acting along the ring's circumference, is accurately captured by dedicated software in Figure 7. The results reflect the surfactant's ability to lower the surface and interfacial tensions, which is essential for improving wetting processes in various applications.

2.6.2. Core Treatment Methods

One is spontaneously imbibed with 2% KCl or 0.1% surfactant solution, and the other is saturated with 2% KCl brine or 0.1% surfactant solution by vacuum.

2.6.3. Optimization of Experimental Methods and Standards

The initial phase of this study involved assessing the interfacial tension and wetting properties of eight distinct surfactant solutions. Three surfactants demonstrating the most favorable profiles characterized by minimal interfacial tension and maximal wetting angles were chosen for subsequent trials. These trials comprised spontaneous imbibition and centrifugation experiments aimed at establishing an effective surfactant system. The selection criteria for the optimal system included the imbibition rate and volume, alterations in water saturation levels, and enhancements in permeability. The comprehensive evaluation furnished a surfactant system optimized for augmenting recovery in reservoirs with restricted permeability, providing a significant advantage in the extraction of hydrocarbons.

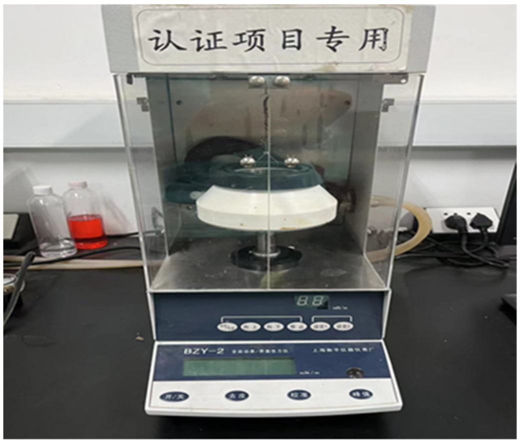

Figure 7. Interfacial tensiometer (model: 16288).

3. Experimental Results and Discussions

3.1. Reservoir Physical Properties

3.1.1. Reservoir Core Characteristics

The formation core samples were taken from Well G24-12#, and the maximum permeability of cores was over 2.0 mD (Table 1), while the minimum permeability was below 0.001 mD. The cores with the high permeability were all fracture cores, while the permeability of matrix cores was generally low.

Table 1. Physical property test results of processed cores.

Core Label	Length/cm	Diameter/cm	Permeability/mD	Porosity/%	Pore Volume/cc	Notes
A	5.031	2.516	2.8230	5.6964	1.424842	fracture core
B	5.003	2.503	0.1035	3.4238	0.842853	
C	4.996	2.487	0.0360	4.093	0.98	
D	4.995	2.505	0.0159	0.9776	0.240667	
E	5.018	2.503	0.0599	4.6964	1.264869	
F	5.003	2.51	1.2100	1.7397	0.4306	fracture core
G	5.006	2.493	0.5204	11.5798	2.8296	fracture core
H	4.987	2.501	0.00025	1.0264	0.2516	
I	5.002	2.428	0.0566	2.6382	0.610988	
J	4.995	2.491	0.0574	14.2224	3.462159	
K	5.003	2.5	0.9847	4.4930	1.215	fracture core

3.1.2. Water and Mineral Analysis of Representative Samples

The core and water samples from Well G24-12# were analyzed. The findings indicated that the produced water is predominantly calcium chloride type with a pH of 6.4, characterized by a high chloride ion content (Table 2).

X-ray diffraction analysis of core samples revealed predominant dolomite compositions exceeding 90%. Layers A–D contain a small amount of quartz, while layers B and D also include calcite; clay minerals were absent in the layers assessed (Table 3).

Table 2. Analysis of representative water samples.

Well Number	Ca^{2+}	K^{+}	Na^{+}	Mg^{2+}	SO_4^{2-}	CO_3^{2-}	Cl^{-}	Total Salinity	Water Type	pH Value
G24-12	115.33	139.27	139.27	34.74	0	0	15,040.37	24,633.94	calcium chloride	6.4

Table 3. Quantitative analysis report of minerals by X-ray diffraction.

Sample Number	Stratum	Mineral Content (%)			
		Quartz	Calcite	Dolomite	Anhydrite
A	MW1 (2, 3)	1.8	0	98.2	0
B	MW1 (2, 3, 4)	2.4	4.9	92.7	0
C	MW2 (4)	2.2	0	91.7	0
D	MW4 (1)	1.6	3.4	93.4	0

3.2. Research on Water-Lock Mechanism of Tight Dolomite

3.2.1. Reservoir Wettability Analysis

Cores C and D were cut into 2.50 cm core slices, respectively, and dried in an oven at 105 °C for 48 h. The "air–water–rock" three-phase contact angle was tested using a contact-angle tester. The results show that the average contact angles are 40.9° and 49.45°, respectively, as depicted in Figure 8. It suggests that the tight dolomite samples are all water-wetting.

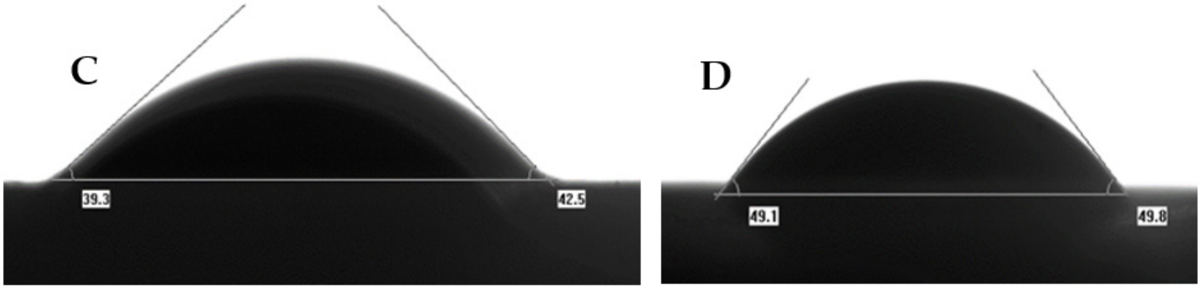

Figure 8. "Air–water–rock" three-phase contact angle of Cores C and D.

3.2.2. Core Permeability with Different Water Saturations

Matrix Core E demonstrated that as water saturation increases, its permeability diminishes exponentially. With water saturation between 10% and 30%, permeability doubles for each 10% reduction in water saturation. Between 30% and 50% saturation, the damage rate drops sharply, with permeability improving by 40% for each 10% reduction in saturation, as shown in Figure 9. This pattern indicates that reduced permeability due to increased water saturation is a primary factor in water-lock damage.

Fractured Core F exhibits significant permeability enhancement with decreasing water saturation: a 50% increase in permeability is observed for each 10% reduction in water saturation between 60% and 70%, and a 70% increase for each 10% decrease from 70% to 85% water saturation, as shown in Figure 10. The presence of fractures likely explains the difference from matrix cores. At lower saturations, as water recedes, large gas channels open, boosting permeability substantially. Further reduction in water saturation has a minor effect as it only releases water from smaller pores, showing minor overall permeability changes. Thus, the permeability of fractured Core F can be notably improved by decreasing water saturation only marginally at high levels.

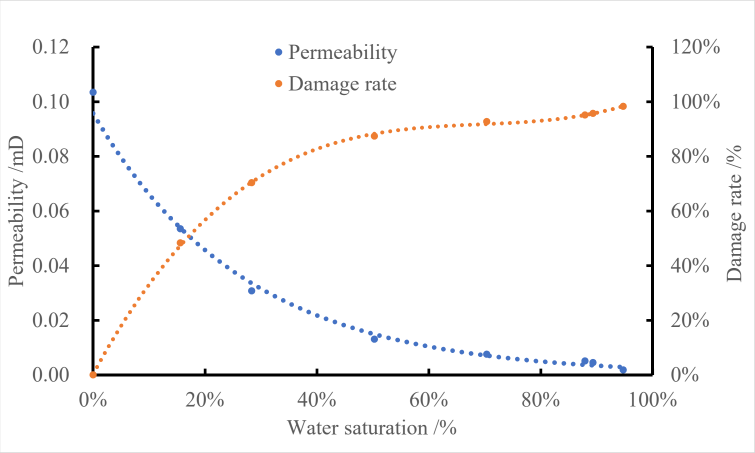

Figure 9. Permeability changes in matrix cores under different water saturations.

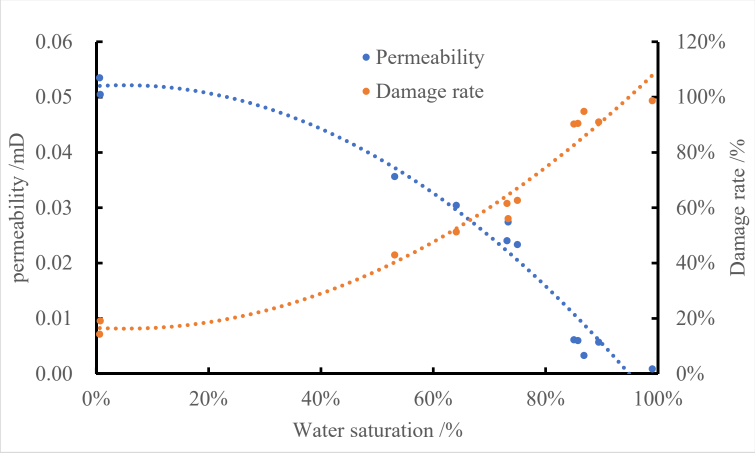

Figure 10. Permeability changes in fractured cores under different water saturations.

3.2.3. Drainage Analysis by Centrifugal Methods

The relationship between relaxation time and pore size satisfies Formula (3) [32]:

$$T_2 = 0.0138D \tag{3}$$

where T_2 is the relaxation time, ms; D is the pore diameter, nm; and the conversion constant is about C = 0.0138 ms/nm. As for the relationship between pore size and relaxation time, it is generally believed that at the inflection point (left and right sides) of the T_2 spectrum curve, the core pores are divided into small pores and large pores [33].

In Figure 11, Core G, characterized by a permeability of 0.52 mD, underwent centrifugation at a rate of 3000 rpm. Observations recorded a reduction in water saturation from 82.8% at the 30 min mark to 59.9% after a period of 120 min, as shown in Figure 12. The initial stages of centrifugation witnessed a pronounced and rapid decrease in water saturation, which slowed over time, eventually stabilizing. Concurrently, the nuclear magnetic resonance signal diminished, with the signal's peak shifting to the right. This shift is indicative of the preferential removal of water from the larger pore spaces within the core. However, the intrinsic water saturation in the core was found to be a mere 24.9% in Figure 12, implying the core's substantial capacity for water absorption under wet conditions.

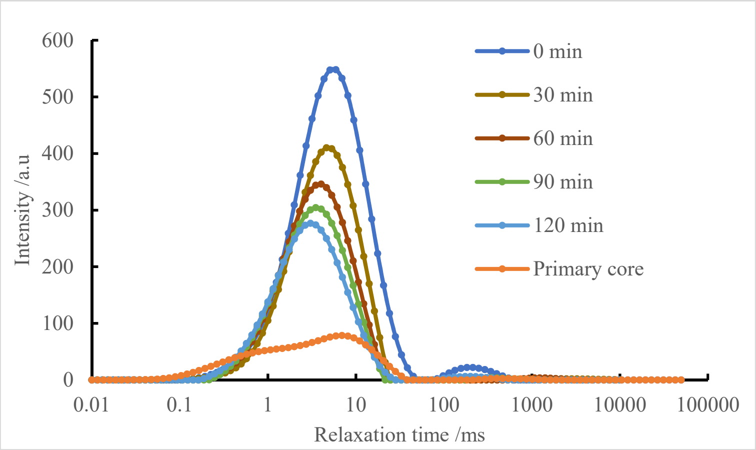

Figure 11. T_2 spectra of Core G at different centrifugation times at 3000 r/min in 2% KCl.

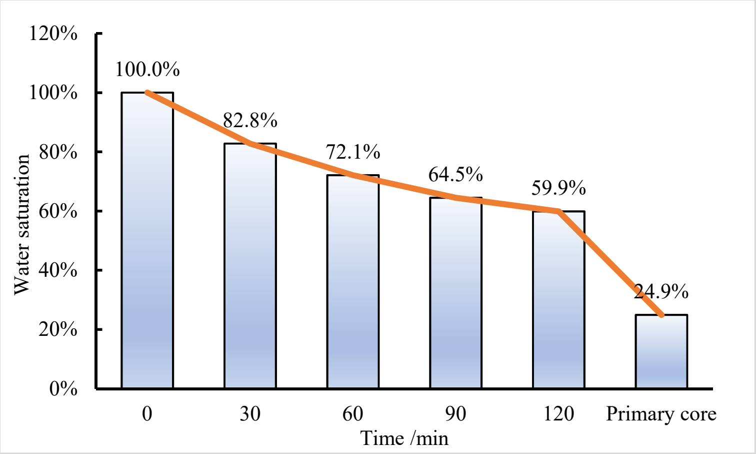

Figure 12. Water saturation in Core G at different centrifugation times at 3000 r/min in 2% KCl.

Core H, which has a low permeability of 0.00025 millidarcies, exhibits a main pore radius of approximately 200 nanometers. In its reservoir state, the core presented an initial water saturation of 56.1%. When subjected to centrifugation at 3000 revolutions per minute for a duration of 30 min, the core exhibited a water expulsion of only 12.8%. Subsequent to this centrifugation process, the nuclear magnetic resonance (NMR) signal showed no significant alterations, indicating that the remaining water saturation was largely irreducible and remained stable at around 83%, as shown in Figures 13 and 14. This suggests that after becoming fully water-saturated, 32.3% of the water within the smaller pores of Core H was not expelled, remaining trapped within the rock matrix, as depicted in Figure 14.

When comparing the centrifugation curves of cores with varying permeabilities under identical centrifugal speeds and times, it is evident that the expulsion of water from both high- and low-permeability cores is restricted. Ultimately, water saturation levels in these cores stabilize, but the rate of decrease in water saturation is more rapid in high-permeability cores than in low-permeability ones, as shown in Figure 15. This pattern reveals that as permeability decreases, the proportion of water that cannot be expelled from the irreducible water saturation increases markedly. This trapped water is a significant factor contributing to the phenomenon of water lock in tight dolomite formations, as it impedes fluid flow and gas recovery, presenting a challenge for production efficiency in such reservoirs.

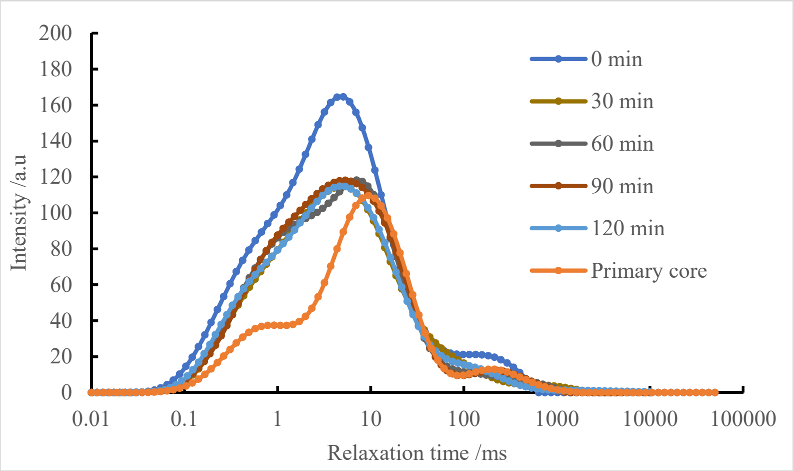

Figure 13. T_2 spectra of Core H at different centrifugation times at 3000 r/min in 2% KCl.

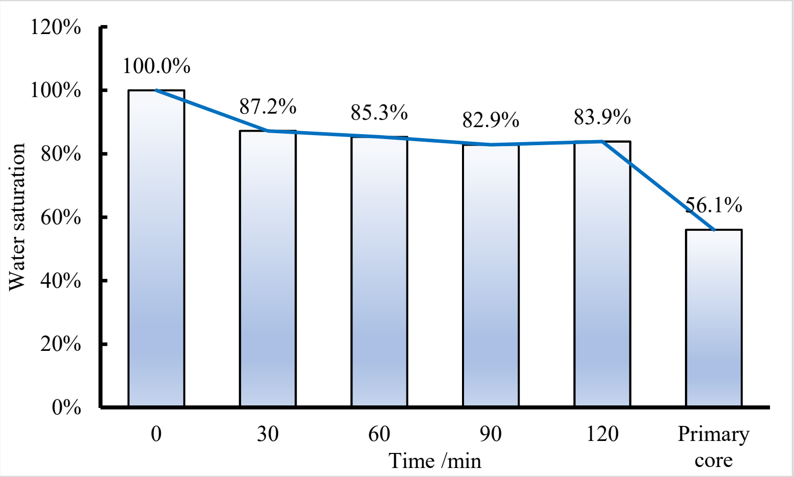

Figure 14. Water saturation in Core H at different centrifugal times at 3000 r/min in 2% KCl.

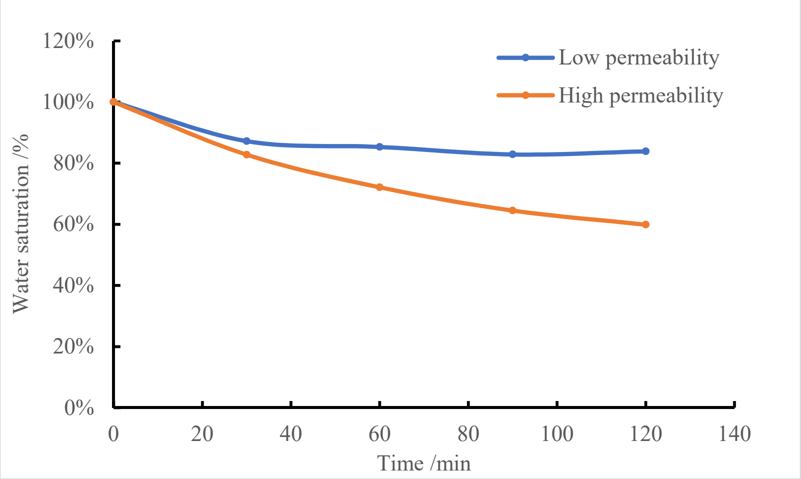

Figure 15. Changes in water saturation with high and low permeability with time.

3.3. Optimization Experiment of Water-Unlocking Reagents

3.3.1. Basic Performance Test of Water-Unlocking Reagents

The surface tension of eight different surfactants at 0.1% concentration was determined (Table 4). One of the main causes of water lock is the capillary force. The greater the capillary force, the more difficult it is to expel water in the pores of rocks, according to Formula (2):

$$P_c = {}^{2\sigma cos\theta}/_{r} \tag{4}$$

Table 4. Surface tension of 0.1% different surfactants.

Surfactants	**Surface Tension mN/m**
AE0-7	27.02
AE0-9	27.75
AM-600	38.45
OP-40	45.78
SDBS	23.62
SDS	29.08
CTAC	33.10
OTAC	37.03

The capillary force is inversely proportional to the surface tension and cosine of the wetting angle.

The smaller the surface tension is, the smaller the capillary force is. Thus, three surfactants, AEO-9, SDBS, and SDS, are selected as follow-up studies.

Core slides were submerged in various 0.1% surfactant solutions for 24 h, followed by a drying process at 105 °C for another 24 h. Subsequent to the drying phase, the "air-water-rock" three-phase contact-angle measurements were performed (Table 5). A larger contact angle corresponds to a lower cosine of the angle, which in turn indicates a reduced capillary force. As a result, two surfactants demonstrating potent efficacy in altering wetting properties were identified as promising water-lock remediation agents.

Table 5. "Water-rock-air" three-phase contact angle after being treated with chemical reagents.

Surfactants	**Average Contact Angle after Treatment/°**
AEO-7	39.65
AEO-9	54.3
AM-600	26.5
OP-40	30.5
SDBS	79.5
SDS	60.55
CTAC	41
OTAC	61.2

The optimal surfactants for modifying surface tension and wetting angles were identified as AEO-9, sodium dodecyl benzene sulfonate (SDBS), and sodium dodecyl sulfate (SDS). To assess water-lock in matrix Core I, the water uptake capabilities of the core were compared using spontaneous imbibition tests in 0.1% solutions of these surfactants. The imbibition curve revealed that within the initial 120 min, the core's spontaneous imbibition rate in the 2% KCl solution outperformed the rates in the other three surfactant solutions. At 200 min, the water saturation in the core was approximately 75% for KCl, while for AEO-9, SDS, and SDBS, the saturations were 68%, 65%, and 58%, respectively, as shown in Figure 16. These results indicate that the introduction of 0.1% SDBS into production wells significantly mitigates spontaneous imbibition and consequently reduces water-lock damage.

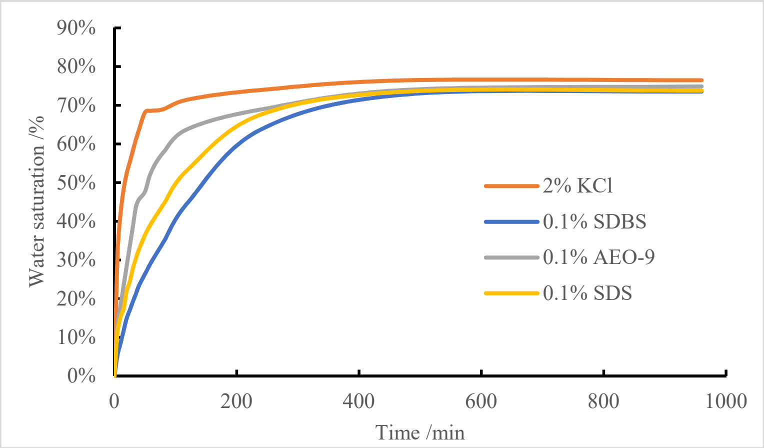

Figure 16. The spontaneous imbibition of cores in 0.1% different chemical solutions.

3.3.2. Efficiency of Water-Unlocking Reagents

Core J was saturated with 0.1% SDBS solution and centrifuged at 3000 r/min. After the saturation process, the initial 20 min of centrifugation led to a rapid decrease in water saturation. As centrifugation proceeded from 20 min to 4 h, the decline in water saturation became progressively slower. After 4 h, the water saturation reduced to 61.3%, which was substantially lower than that achieved using the 2% KCl solution, as shown in Figures 17 and 18. These results suggest that SDBS is effective at mitigating water-lock issues in reservoir cores.

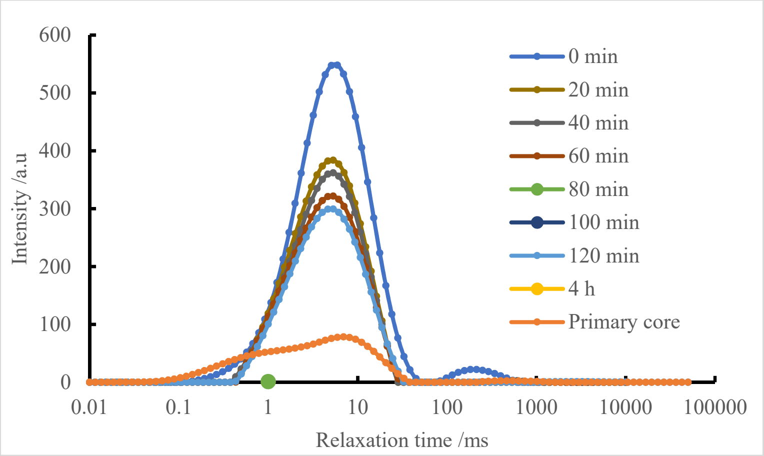

Figure 17. T_2 spectra of Core J treated with 0.1% SDBS at different centrifugal times.

When comparing the centrifugal drainage efficiency of a rock before and after the addition of 0.1% SDBS under identical centrifugal force and duration, the introduction of SDBS enhances water expulsion from the rock, resulting in higher discharge efficiency. Specifically, the use of SDBS increased the drainage rate by 15.7% at 20 min and by 14.27% at 4 h of centrifugation, as shown in Figure 19. This indicates SDBS's effectiveness in improving water removal from reservoir rocks.

For fractured Core K, the initial 30 min of centrifugation primarily expels water from fractures, with minimal discharge from the fine pores at the core's periphery. From 30 to 60 min, as centrifugation persists, water redistributes from larger to smaller pores, which is evidenced by minimal changes in the total peak area from nuclear magnetic resonance

(NMR) measurements shown in Figures 20 and 21. This behavior indicates that water expulsion in fractured cores predominantly takes place within the fractures.

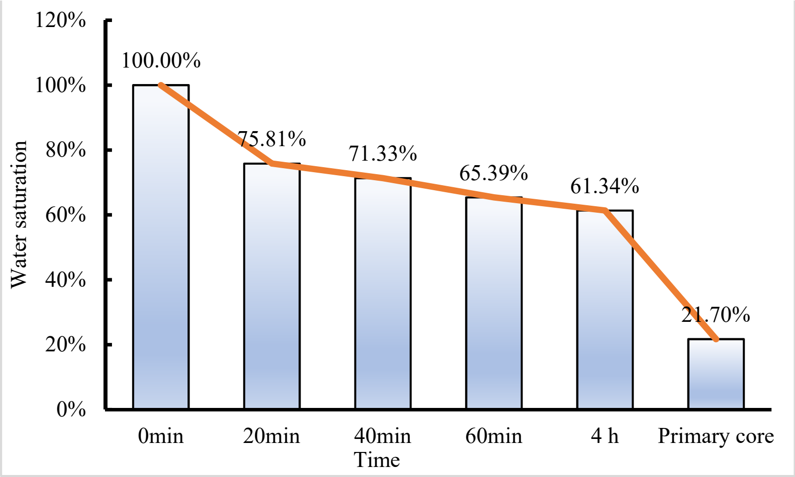

Figure 18. Water saturation in Core J treated with 0.1% SDBS at different times and 3000 r/min.

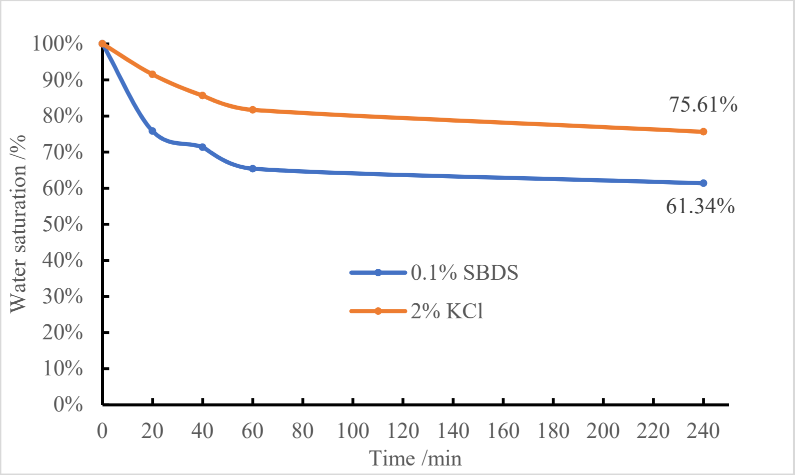

Figure 19. Water saturation with centrifugation time before and after SDBS treatment.

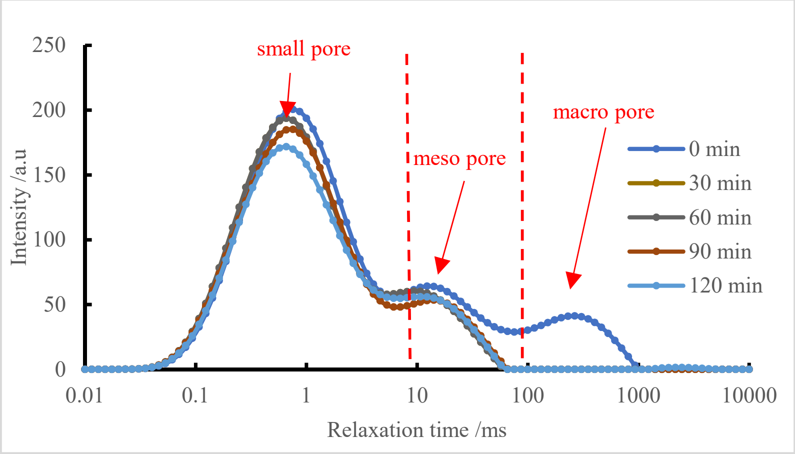

Figure 20. T_2 spectra of fractured core with different centrifugal times in 2% KCl.

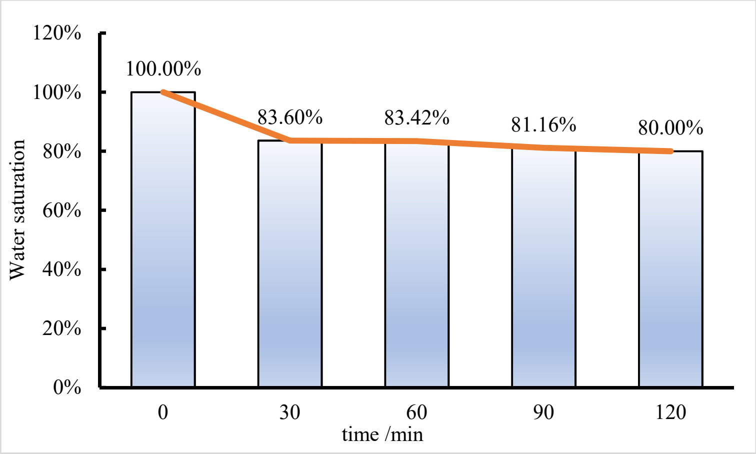

Figure 21. Water saturation in fractured cores with different centrifugal times in 2% KCl.

The drainage pattern of the fractured core saturated with 0.1% SDBS after centrifugation mirrors that of the core saturated with saline water. Following a two-hour centrifugation period, the final water saturation level settles at 76.9%, which is 3.1% lower than that of the matrix core, as shown in Figures 22 and 23. This indicates that while fractures serve as pathways for fluid flow, they are not effective in alleviating water lock within the matrix.

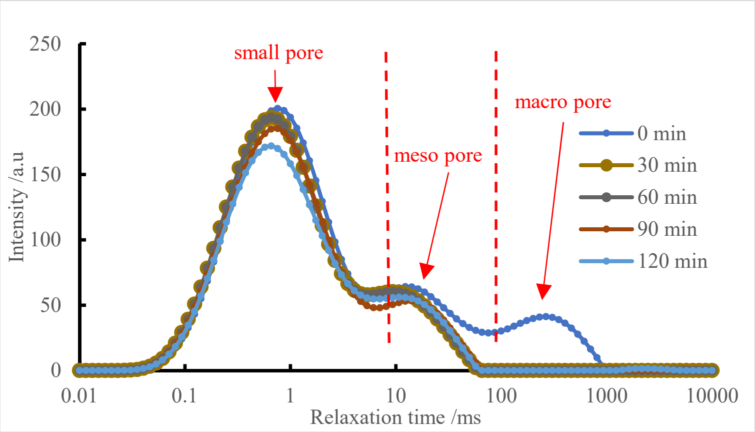

Figure 22. T_2 spectra of fractured core with centrifugal times after 0.1% SDBS solution.

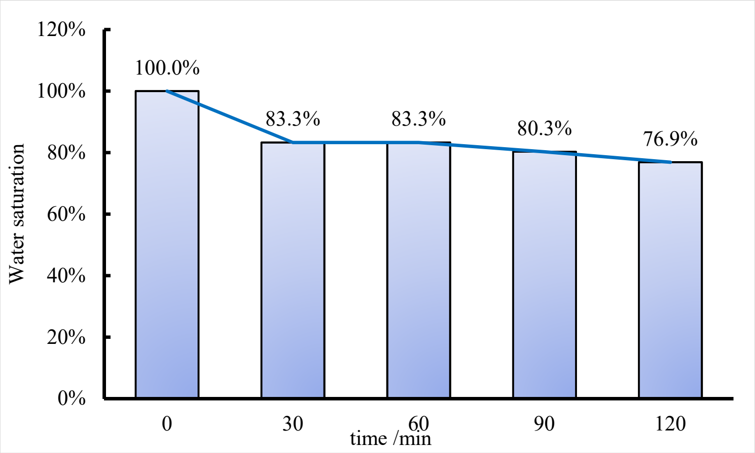

Figure 23. Water saturation in fractured core with centrifugal times after 0.1% SDBS solution.

4. Conclusions

(1) The Ordos Basin's Lower Paleozoic Ordovician strata are primarily dolomitic, with a high formation water salinity. The porosity of these tight reservoirs ranges from 1.25% to 9.50%, and permeability varies from 0.001 mD to 7.1 mD, leading to a predisposition for water-lock damage due to their low-porosity and low-permeability characteristics. The reservoir's strong affinity for water absorption, evidenced by an average wetting contact angle below 50° and original water saturation levels between 21.7% and 56.1%, leads to approximately 75% water saturation after spontaneous imbibition. This strong imbibition capacity is a significant contributor to water-lock damage.

(2) There is a clarified relationship between permeability and water saturation in the reservoir. For both matrix and fractured core types, the relationship between water saturation and gas permeability is described by different exponential trends. Notably, gas permeability increases substantially by at least 40% for each 10% decrease in water saturation below 70%, indicating that water saturation critically affects water-lock damage. Centrifugal drainage experiments show that cores with higher permeability exhibit a quicker reduction in water saturation over the same centrifugation period compared to those with lower permeability. Moreover, high permeability cores reach a lower final irreducible water saturation, highlighting that reduced permeability significantly elevates irreducible water saturation, which is a prominent cause of water lock in tight dolomite.

(3) From an initial selection of eight surfactants, three were optimized based on their ability to alter interfacial tension and wettability. The surfactant 0.1% SDBS is highlighted for its slow imbibition rate and extended equilibrium time, making it an effective agent for addressing water lock in tight dolomite formations. The modification of cores with a 0.1% SDBS solution leads to improved centrifugal drainage in both matrix and fractured core types. Although the drainage enhancement is observed in both, the effect is less marked in fractured cores because fractures act as conduits for gas flow, which does not assist in alleviating matrix water lock as effectively.

Author Contributions: Investigation, D.G.; Resources, X.Y., J.S. and D.G.; Data curation, L.S.; Writing—original draft, X.Y., H.F. and L.S.; Writing—review & editing, E.Y. All authors have read and agreed to the published version of the manuscript.

Funding: The authors declare that this study received funding from National Natural Science Foundation of China (Grant No. 52004306), the Strategic Cooperation Technology Projects of CNPC and CUPB (Grant No. ZLZX2020-01 and ZLZX2020-02)and the National Science and Technology Major Projects of China (Grant No. 2016ZX05030005, 2016ZX05051003).

Data Availability Statement: Data are contained within the article.

Conflicts of Interest: Xiaopeng Yang, Junfeng Shi, Donghong Guo and Erdong Yao were employed by the company PetroChina Company Limited. The remaining authors declare that the research was conducted in the absence of any commercial or financial relationships that could be construed as a potential conflict of interest.

References

1. Branco, F.R.; Gil Natália, A.; Trevisan, O.V. NMR study of carbonates wettability. *J. Pet. Sci. Eng.* **2017**, *157*, S0920410517305223. [CrossRef]
2. Zou, C.; Zhai, G.; Zhang, G.; Wang, H.; Zhang, G.; Li, J.; Wang, Z.; Wen, Z.; Ma, F.; Liang, Y.; et al. Formation, distribution, potential and prediction of global conventional and unconventional hydrocarbon resources. *Pet. Explor. Dev.* **2015**, *42*, 14–28. [CrossRef]
3. Al-Rubaiyea, J.; Al-Houli, M.; Al-Ajmi, F.; Al-Duwaish, M.; Elsherif, A.; Lahmar, H. Establishing Mobility Profile in a Carbonate Reservoir Using LWD Imaging Technology, A Case Study From Partitioned Zone Between Kuwait and Saudi Arabia. In Proceedings of the Spe Kuwait Oil & Gas Show & Conference, Mishref, Kuwait, 11–14 October 2015. [CrossRef]
4. Xinhua, M.A.; Yu, Y.; Long, W.; Luo, B. Distribution and exploration direction of medium-and large-sized marine carbonate gas fields in Sichuan Basin, SW China. *Pet. Explor. Dev.* **2019**, *46*, 1–15. [CrossRef]
5. Li, X.; Guo, Z.; Hu, Y.; Luo, R.; Su, Y.; Sun, H.; Liu, X.; Wan, Y.; Zhang, Y.; Li, L. Efficient development strategies for large ultra-deep structural gas fields in China. *Pet. Explor. Dev.* **2018**, *45*, 118–126. [CrossRef]

6. Yang, S.R.; Schultheis, A.M.; Yu, H.; Mandelker, D.; Ladanyi, M.; Büttner, R. Characteristics and genetic types of the Lower Paleozoic natural gas, Ordos Basin. *Mar. Pet. Geol.* **2017**, *76*, 67–69. [CrossRef]
7. Liu, X.; Liu, Y.; Chen, J. Microscopic pore structure and seepage characteristics of tight sandstone gas reservoirs in Member 8 of Hehe Formation, Ordos Basin. *Nat. Gas Geosci.* **2016**, *7*, 672–1926.
8. Lu, T.; Liu, Y.; Wu, S. Difficulties and countermeasures in stabilizing production of tight sandstone gas reservoir in Sulige Gas Field, Ordos Basin. *Nat. Gas Ind.* **2015**, *35*, 43–51.
9. Wang, C.; Su, Y.; Wang, W.; Li, L.; Zhang, L.; Wang, T. Water Blocking Damage Evaluation and Mitigation Method in Tight Gas Reservoirs. *Energy Fuels* **2022**, *36*, 10934–10944. [CrossRef]
10. Geng, J.; Yan, J.; Li, Z. Mechanisms and prevention of damage for formations with low-porosity and low-per-meability. In Proceedings of the International Oil and Gas Conference and Exhibition in China, Beijing, China, 8–10 June 2010; SPE 130961.
11. Shu, Y.; Yan, J. New fluids prevent formation damage to Tarim sandstones. *Oil Gas J.* **2008**, *106*, 45–49.
12. Bahrami, H.; Rezaee, R.; Clennell, B. Water blocking damage in hydraulically fractured tight sand gas reservoirs: An example from Perth Basin, Western Australia. *J. Pet. Sci. Eng.* **2012**, *88–89*, 100–106. [CrossRef]
13. Civan, F. *Reservoir Formation Damage*, 2nd ed.; Springer: Berlin/Heidelberg, Germany, 2007; pp. 937–984. [CrossRef]
14. Bennion, D.B.; Thomas, F.B.; Ma, T. Formation Damage Processes Reducing Productivity of Low Permeability Gas Reservoirs. In Proceedings of the SPE Rocky Mountain Regional/Low-Permeability Reservoirs Symposium and Exhibition, Denver, CO, USA, 12–15 March 2000. [CrossRef]
15. Ghalambor, A.; Lafayette, U.O.L.A.; Economides, M.J. Formation Damage Abatement: A Quarter-Century Perspective. In Proceedings of the SPE International Symposium on Formation Damage Control, Lafayette, LA, USA, 23–24 February 2000.
16. Su, X.; Wang, Q.; Song, J.; Chen, P.; Yao, S.; Hong, J.; Zhou, F. Experimental study of water blocking damage on coal. *J. Pet. Sci. Eng.* **2017**, *156*, 654–661. [CrossRef]
17. Liu, S.; Dou, X.; Zeng, Q.; Liu, J. Critical parameters of the Jamin effect in a capillary tube with a contracted cross section. *J. Pet. Sci. Eng.* **2020**, *196*, 107635. [CrossRef]
18. Zhang, L.; Zhou, F.M.; Wang, J.; Wang, J.; Zhang, J.; Shi, C. Research on sensitivity damage of naturally fractured carbonate reservoirs in Ordos Basin. *Arab. J. Geosci.* **2019**, *12*, 595. [CrossRef]
19. Zhang, X.; Dang, B.; Wang, X.; Luo, S.; Chen, B.; Zheng, L. Acid-Soluble Drilling Fluid in the Northern Carbonate Reservoir of the Yishan Slope in the Ordos Basin. *Energies* **2023**, *16*, 6020. [CrossRef]
20. Fan, H.; Lyu, J.; Zhao, J.; Zhao, S.; Fan, H.; Geng, J.; Dai, C.; Kang, W. Evaluation method and treatment effectiveness analysis of anti-water blocking agent. *J. Nat. Gas Sci. Eng.* **2016**, *33*, 1374–1380. [CrossRef]
21. Liao, R.; Xu, Y.; Hu, X. Damage to low-permeability reservoir by water locking effect and its inhibiting and removing methods. *Nat. Gas. Ind.* **2002**, *22*, 87–89.
22. Lu, Y.; Li, H.; Lu, J.; Shi, S.; Wang, G.; Ye, Q.; Li, R.; Zhu, X. Cleaning up water blocking in gas reservoirs by microwave heating. *J. Pet. Technol.* **2015**, *59*, 76–81.
23. Ni, G.; Cheng, W.; Lin, B.; Zhai, C. Experimental study on removing water blocking effect (WBE) from two aspects of the pore negative pressure and surfactants. *J. Nat. Gas Sci. Eng.* **2016**, *31*, 596–602. [CrossRef]
24. Zhao, D.; Zheng, W.; Liu, Y. Experimental study on reducing water lock effect of low permeability gas reservoir by alcohol treatment. *J. Southwest Pet. Inst.* **2004**, *26*, 67–69.
25. Liu, X.; Kang, Y.; Luo, P.; You, L.; Tang, Y.; Kong, L. Wettability modification by fluoride and its application in aqueous phase trapping damage removal in tight sandstone reservoirs. *J. Pet. Sci. Eng.* **2015**, *133*, 201–207. [CrossRef]
26. Feng, C.; Kong, Y.; Jiang, G. Research on water block removal by wettability alteration to gas-wetting in condensate reservoir. *Drill. Fluid Complet. Fluid* **2011**, *28*, 1–4.
27. Aminnaji, M.; Fazeli, H.; Bahramian, A.; Gerami, S.; Ghojavand, H. Wettability alteration of reservoir rocks from liquid wetting to gas wetting using nanofluid. *Transp. Porous Media* **2015**, *109*, 201–216. [CrossRef]
28. Li, Y.; Zhou, F.; Wang, J.; Li, B.; Xu, H.; Yao, E.; Zhao, L. Influence of Nanoemulsion Droplet Size of Removing Water Blocking Damage in Tight Gas Reservoir. *Energies* **2022**, *15*, 5283. [CrossRef]
29. Wang, Y.; Jin, J.; Ma, L.; Li, L.; Zhao, X. Influence of wettability alteration to preferential gas-wetting on displacement efficiency at elevated temperatures. *J. Dispers. Sci. Technol.* **2015**, *36*, 1274–1281. [CrossRef]
30. Bennion, D.B.; Thomas, F.B.; Bietz, R.F.; Bennion, D.W. Water and hydrocarbon phase trapping in porous media-diagnosis, prevention and treatment. *J. Can. Pet. Technol.* **1996**, *35*, 10. [CrossRef]
31. Li, K.; Firoozabadi, A. Experimental study of wettability alteration to preferential gas-wetting in porous media and its effects. *SPE Reserv. Eval. Eng.* **2000**, *3*, 139–149. [CrossRef]
32. Liu, Y.; Yao, Y.; Liu, D.; Zheng, S.; Sun, G.; Chang, Y. Shale pore size classification: An NMR fluid typing method. *Mar. Pet. Geol.* **2018**, *96*, 591–601. [CrossRef]
33. Hinai, A.A.; Rezaee, R.; Esteban, L.; Labani, M. Comparisons of pore size distribution: A case from the Western Australian gas shale formations. *J. Unconv. Oil Gas Resour.* **2014**, *8*, 1–13. [CrossRef]

Disclaimer/Publisher's Note: The statements, opinions and data contained in all publications are solely those of the individual author(s) and contributor(s) and not of MDPI and/or the editor(s). MDPI and/or the editor(s) disclaim responsibility for any injury to people or property resulting from any ideas, methods, instructions or products referred to in the content.